

Nanolubrication

J.L. Mansot, Y. Bercion, L. Romana

Groupe de Technologie des Surfaces et Interfaces (GTSI EA 2432), Université des Antilles et de la Guyane, UFR Science Exactes et Naturelles Pointe à Pitre Cédex Guadeloupe (FRANCE)

J.M. Martin

Laboratoire de Tribologie et Dynamique des Systèmes (LTDS UMR 5513), Ecole Centrale de Lyon, 36 avenue Guy de Collongue, 69134 Ecully cédex (FRANCE)

(Received on 1 July, 2008)

Lubrication strategies developed long time ago employed amphiphilic molecular lubricant additives to confer to lubricating oils or greases specific properties such as friction reduction, antiwear, anticorrosion. The understanding of their action and the development of various type of nanoparticles are at the origin of new lubrication strategies using composite or functionalized nanoparticles in dispersion in lubricating oils or greases to confer to the lubricants the needed functions. The present work is concerned with the presentation of these new approaches. Some examples will be developed to show the main aspects of the mechanisms of action of these new nano-additives.

Keywords: tribology, colloidal additives, reverse micelles, nanoparticles

I. INTRODUCTION

Tribology has been introduced in early humanity ages [1] as far as, during stone age, contact mechanics is involved in the cutting and polishing of flints and friction between two flints or two wood peaces is used for fire ignition. An Egyptian bas-relief, found in the Tehuti-Hetep's grave (1880 BC), is probably one of the first documents reporting the use of lubricant (water or oil) to reduce friction between the sleigh, used for a 60 tons statue transportation, and the boards on which it slides.

The two basic laws of friction, expressing that friction resistance is proportional to normal load and independent on the contact area between solids, seem to be first mentioned by Leonardo da Vinci (1452-1519) and rediscovered by Guillaume Amontons in 1699 [2]. These observations were verified, in 1785, by Charles Augustin Coulomb [3]. He did the distinction between static friction (force needed to start sliding between two solids) and kinetic friction (force required to maintain sliding). The Coulomb expression for the friction coefficient μ , already used today, is the ratio between friction force F_F and the normal load F_N applied to the contacting solid bodies (figure 1). He experimentally observed, for dry sliding, that friction is nearly independent of the sliding speed and considered that friction can be due to molecular adhesion of surfaces and contacts between asperities. The elastic contact theory published by Hertz in 1882 [4, 5] developed the calculations of the pressure distribution in the contact and revealed the high values of this parameter even in a weak loaded contact (figure 1). In 1902 Richard Stribeck [6] introduced a curve (figure 2) which allowed to distinguish various lubrication regimes (boundary, mixte, elasto hydrodynamic and hydro dynamic lubrication regimes) mainly depending on the normal applied load to the contact, the sliding speed and the viscosity of the lubricant. The more severe regime, the boundary one, is characterized by the absence of lubricant film in the sliding interface leading to contact between surface asperities of the solid bodies as mentioned in the Coulomb model. Sir William B. Hardy [7] was the first to investigate, in the beginning of the 20th century the role of hydrocarbon molecules on static friction (boundary regime).

He pointed out the important role of molecular layers (boundary layers) adsorbed on the solid surfaces. It was probably the first controlled introduction of nano-objects (amphiphilic molecules) in a sliding interface. Stimulated by the Hardy's results lot of researches started on boundary film physics and chemistry resulting in the development of molecular theories of lubrication and leading to the design of lubricant additives allowing lubricating oils and greases to improve the yield and the durability of mechanical devices by reducing both friction and wear [8-19].

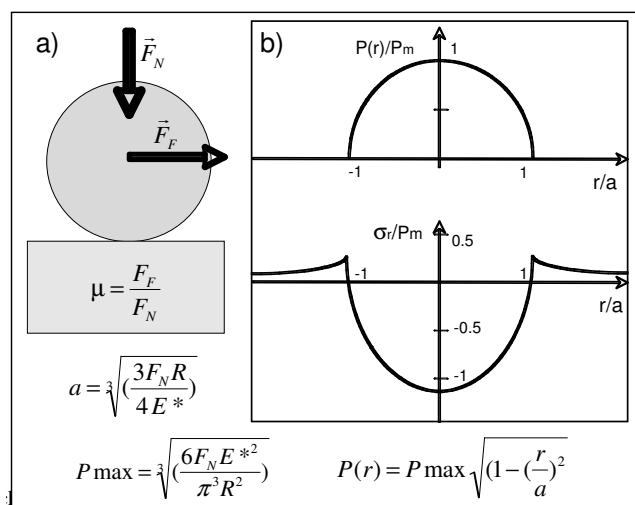


FIG. 1: **a)** Schematic representation of an elastic sphere on plane contact showing the friction F_F and normal F_N forces applied to the contacting solid bodies which define the friction coefficient μ . **b)** Distributions of pressure $P(r)$ and radial stress $\sigma(r)$ in the contact area as a function of the distance r to the contact centre deduced from Hertz Theory [4,5]. Hertz's mathematical expressions for: the contact area radius a , the pressure as a function of contact parameters (normal applied load F_N , reduced Young's modulus E^* and ball radius R). A rapid calculation in the case of a contact between a sphere of 5 mm radius and a plane both made of AISI 52100 steel ($E^* = 110GPa$) under a normal load of 12 N lead to a maximal pressure of 1 GPa for a contact radius of 76 μm .

The present paper will be more specifically concerned with

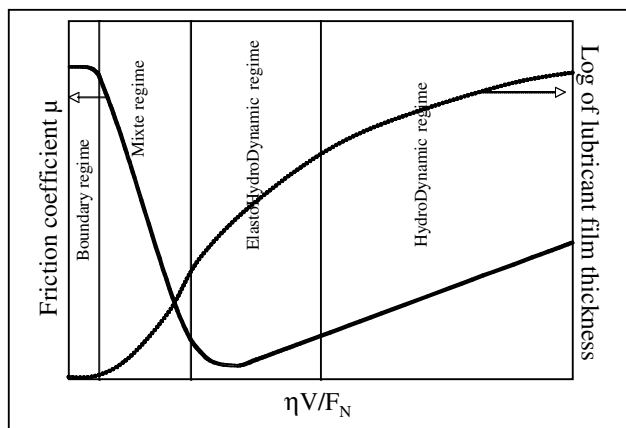


FIG. 2: Schematic Stribeck's Curve (μ and $\text{Log } h$) as a function $\eta V/F_N$ of (F_N normal applied load, V sliding speed and η lubricant viscosity). The boundary lubrication regime corresponds to the severe one with high friction coefficients (μ) and low lubricant film thicknesses (h) values.

the boundary lubrication regime where high friction coefficients and severe wear are recorded. We will first make a brief overview on the action mechanisms of conventional friction reducers and anti-wear lubricant additives. From the main results we will introduce the nano-lubrication approaches mainly based on the use of dynamic or static nanoparticles. Examples of such additives will then be treated to illustrate these new strategies.

Introduction to the experimental device for friction and wear studies in the boundary regime

In order to measure friction and wear specific devices, called tribometers, are used.

The schematic representation of the alternative sphere on plane tribometer, used for the second part of the paper, is presented in figure 3. Depending on the tribometer, the contact geometry can be sphere / plane, cylinder /plane, cylinder /cylinder or plane/plane. In the case of the sphere plane/contact geometry adjustment of the contact is easy and high pressures are generated in the contact (1GPa) for relatively small normal applied load (12N).

Measurement of the friction coefficient

Depending of the system, the normal load can be applied by a mass deposited onto the arm of the tribometer or by an elastic device (spring...). The normal and friction forces are measured either by piezo electric transducers or strain gauges devices. Control of the tribometer, data acquisition and treatments are done using computer.

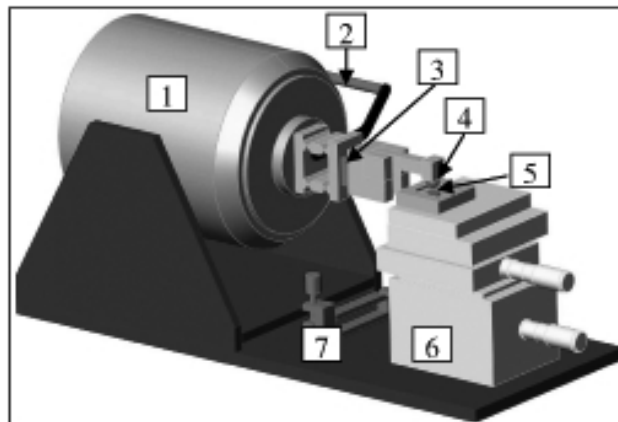


FIG. 3: Schematic representation of an alternative sphere/plane tribometer. (1) motor, (2) displacement transducer, (3) triaxial force transducer, (4) sphere, (5) plane, (6) x,y,z adjustable sample holder, (7) elastic device for normal load application.

Overview on action mechanisms of conventional additives in boundary lubrication regime

Friction reduction by "unctuous" additives

First introduced by Hardy [7] the unctuous additives are amphiphilic molecules such as organic acids. The systematic study of friction reduction action of monolayers for various molecules was done by W.A. ZISMAN [8]. He points out the relationship between the boundary friction coefficient and the monolayer thickness adsorbed on the sliding surfaces. He especially demonstrated, in the case of linear fatty acids, that the friction coefficient decreases as a function of the monolayer thickness (molecular length) tending to an asymptotic value of 0.1 for acids larger than dodecanoic acid. These results led to a monomolecular layer lubrication model. Recent studies on molecular friction allowed the authors [20-21] to establish a quantitative relation between the friction coefficient and the molecular film thickness which can be expressed in the following form:

$$\mu = \mu_0 + \kappa/h^n \quad (1)$$

μ is the measured friction coefficient, μ_0 and κ are friction coefficient and parameter intrinsic to the molecules constituting the monolayer, h is the thickness of the layer in the contact conditions and n an exponent experimentally found between 3 and 5.

Theoretical approaches implying either atomic scale stick-slip motions [22-23] or electro-dynamic interactions between sliding surfaces generated during sliding [24] were developed. The last one leading to an exponent value $n=4$ in the expression (1).

However it is important to note that after few cycles of friction such mono-layers are destroyed either by bonds breakings or chemical reactions with the contacting surfaces leading to the built up of new interface materials (with physical properties and thickness different from the initial monolayer [26]) and finally its progressive elimination from the sliding contact. If the molecular layer is formed from a dispersion of

molecules into an hydrocarbon base oil embedding the sliding contact, the friction can remain stable at a relatively low value as far as continuous adsorption of amphiphilic molecules on the sliding surfaces occurs [27].

Antiwear additive action mechanisms

In the boundary lubrication regime, the action of conventional anti-wear additives occurs via the built up of a tribologic film. This one results from the chemical reaction between the additive molecules and the sliding surfaces in contact [10 - 12]. The case of Zinc Dialkyl DithioPhosphate (ZDDP) additive has been extensively studied by Analytical Transmission Electron Microscopy (ATEM). The morphology, nature, structure and tribologic properties of the tribochemical film were obtained [9 - 14]. The main results are presented in figures 4 and 5.

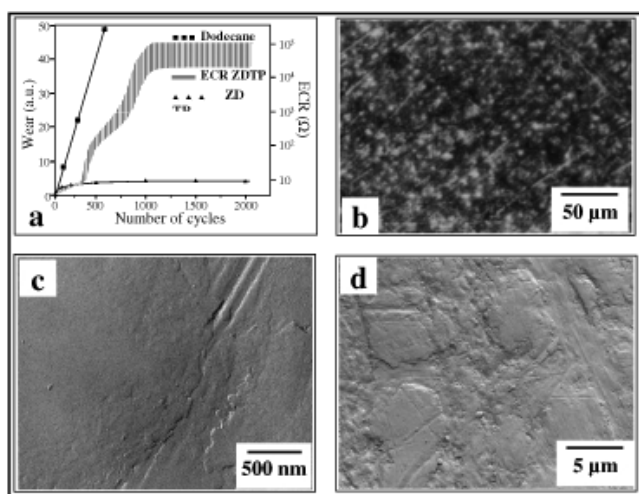


FIG. 4: Results of plane (AISI 52100 steel) on plane (cast iron) friction test at 80 °C in the presence of 1% ZDTP in dodecane solution. (a) Evolution of Electrical Contact Resistance (ECR) and wear rate as a function of number of cycles. As it can be seen, the establishment of the anti wear film needs an induction period where the wear rate is as high as with pure oil base (dodecane curve). The built up of the insulating tribologic film is pointed out by the increase of the ECR which is correlated to the decrease of the wear rate. (b) Visible light micrograph of the worn surface recorded at the end of the test. It reveals the presence of the blue insulating anti wear film. (c), (d) TEM micrographs recorded on platinum shadowed carbon replica showing the morphology of the surface film. The platelets (~ 50 nm thick) correspond to the blue areas seen in the optical micrograph. The presence of the anti wear film onto the sliding surfaces avoids direct metal / metal contacts

Complementary structural and analytical studies of the tribologic films using Auger Electron Spectroscopy (AES), X ray Photo-electron Spectroscopy (XPS) and X ray Absorption Near Edges Structures (XANES) [15, 16] reveal that the chemical reaction involved for the built up of the film in the physical contact conditions (pressure raising 1 GPa and shear stress of 10^5 s $^{-1}$) are readily different from thermal degradation. These results were recently interpreted with new theoretical approaches (Hard and Soft Acid-Base theory) [17,19].

The collected results lead to an accurate description of the anti-wear film schematized in figure 6. This one is mainly composed of amorphous Fe/Zn poly(thio)phosphate embedding some nano-crystallites of ZnO, ZnS.

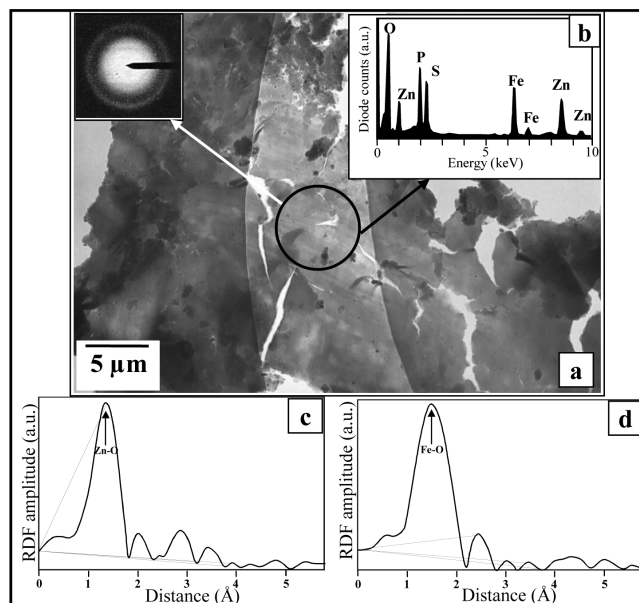


FIG. 5: (a) TEM image recorded onto an anti-wear film particle and corresponding electron diffraction pattern. (b) X ray spectrum (EDXS). The anti-wear film is composed of iron (from contacting surfaces) and elements present in the ZDDP additive (O, P, S, Zn) [11, 12]. (c) and (d) Fe and Zn Radial Distribution Functions (RDF uncorrected from phase shifts) extracted from EXAFS experiments on ZDDP anti-wear film particles [13, 14]. The electron diffraction pattern and the presence of one major peak in each RDF, corresponding to oxygen first neighbour shells, point out the amorphous structure of the anti-wear film.

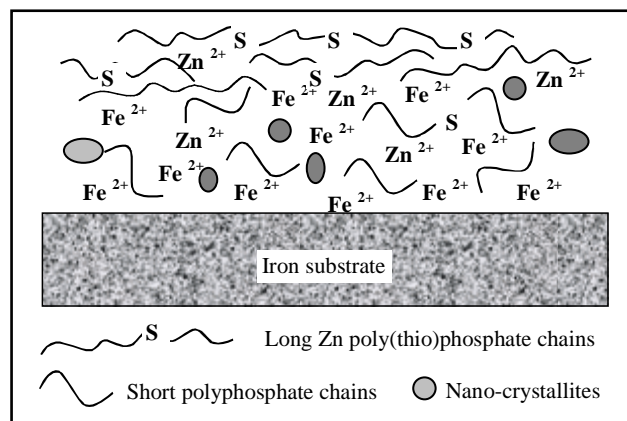


FIG. 6: Schematic structure of the ZDDP tribo-film according to the multi techniques approaches [16]

Although ZDDP revealed itself as a highly efficient anti-wear additive during the last decades, its action mechanism presents however two disadvantages:

1. As shown on the wear rate and electrical contact resis-

tance versus number of cycles diagram (figure 4) the anti-wear action of ZDDP requires an induction period for the built up of the tribo-chemical film. During this period the wear rate is as high as additive free oil.

2. The development and use of new materials for various mechanical applications presenting weak chemical reactivity with conventional (ZDDP) additives do not allow the built up of the anti-wear film.

An alternative way based on the use of nano-sized particles of tribologic film precursors is now proposed to build up the protective tribologic film without chemical reaction of the additive with the contacting surfaces.

The Nanolubricant approach

The nanolubricant approach is used to overcome the disadvantages of conventional anti-wear and friction reduction additives related to their need of chemical reactions with substrates and the resulting induction period to produce the tribo-film on sliding surfaces.

The strategy is based on the direct feeding of the sliding interface with nano-particles of tribo-active phases (graphite, MoS_2 , fluorinated carbon species [28-30]) or precursors of tribo-active phases (precursor of lamellar phases such as, carbon nano-onions or nanotubes, metal dichalcogenide fullerenes, ... [31-35]) dispersed in lubricant base oils or greases to produce the tribo-film without reaction with the substrate surfaces. The main advantages of nano-particles are their sizes, in the nano-meter range, which is well adapted for a perfect feeding of the sliding interface and the possibilities of composite particle syntheses which can combine multiple properties such as friction reduction, anti-wear anticorrosion...

An other route, using nano-particles of two different reagents needing contact physical conditions to react has been successfully tested but with material presenting weak interest for tribologic applications [36].

In the following part of the paper two types of nano-particles will be used to illustrate the nano-lubricant approach: dynamic metal soap micelles, synthesized encapsulated particles (stable reverse micelles). The structure of the initial nano-materials and final tribo-film will be investigated and correlated to the tribologic behaviour. Mechanisms of action will be proposed.

Organometallic Reverse micelles and mineral encapsulated nano particles

Dynamic soap micelles

Soap molecules, resulting from reaction between organic acids and mineral bases (metal hydroxides, metal carbonates...) are amphiphilic molecules (figure 7). When such molecules are introduced in non-polar media (mineral oils or non-polar solvents), they aggregate into reverse micelles in equilibrium with single molecules present in the solvent at the Critical Micellar Concentration (CMC) [37-39]. In the case

of spherical reverse micelles the classical core / shell structure will be obtained (mineral hydrophilic groups in the micelle's cores and non-polar chains in the shell). The molecular interactions responsible of aggregation are of physical nature (van der Waals, Coulombian, hydrogen bonding...). The reversible character of these bonding types confers to such aggregates their dynamic behaviour.

Depending on the solvent, the molecular concentration, the temperature and the pressure, the micelles can adopt various shapes and sizes with various numbers of aggregated molecules. For example, in the same solvent, at constant pressure and temperature, from lowest (just above the CMC) to highest concentrations micelles will evolve from spherical shape to cylinders, wormlike micelles (long flexible cylinders) and lamellar assemblies (figure 7) [37, 39].

Characterization of the CMC, the size, the shape, the number of molecules by aggregates in such micellar dispersions can be achieved using Quasi Elastic Light Scattering (QELS) [40, 41]. In some cases, Transmission Electron Microscopy (TEM) coupled to the freeze fracturing and etching technique (FFET) [39-42] can advantageously be used to visualize micelles shape, size and dispersion in the continuous phase (figure 8) [21].

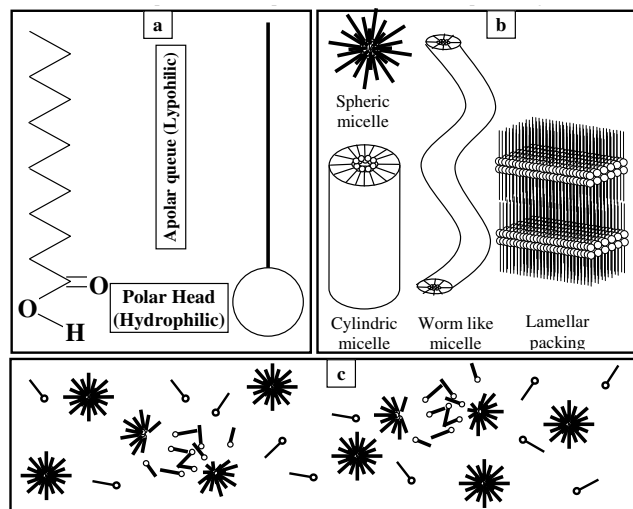
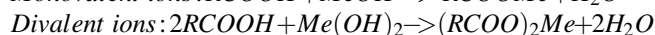
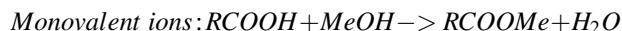


FIG. 7: (a) Typical amphiphilic molecule (organic acid molecule) and classical simplified representation. (b) Various types of molecular aggregations. (c) Schematic representation of the dynamic character of the micellar aggregates in equilibrium with single molecules dispersed at the CMC in the solvent.

Depending on the metal atom valence and on the synthesis process, various types of soap molecules can be obtained.

In the case of stoichiometric also called neutral soap, soap molecules syntheses will correspond to the following reactions [43, 44]:



In the formula, Me represents the metal atom.

The organic acids $RCOOH$, where R is an hydrocarbon chain, can be replaced by alkyl sulphuric acids ($ROSO_3H$), alkyl aryl sulfonic acids (RSO_3H), alkyl phenols (ROH) (see figure 9). In the case of divalent ions, non-stoichiometric also called

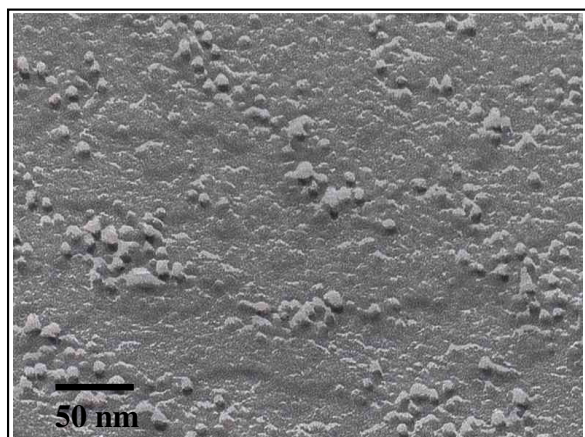


FIG. 8: Aspect of polymeric micelles (viscosity index improver and friction reducer [21, 40]) in dodecane as observed by means of transmission electron microscopy on a platinum shadowed replica prepared by the freeze fracturing technique. Micelles appear as spherical particles with a diameter around 6 nm (confirmed by quasi elastic light scattering experiments).

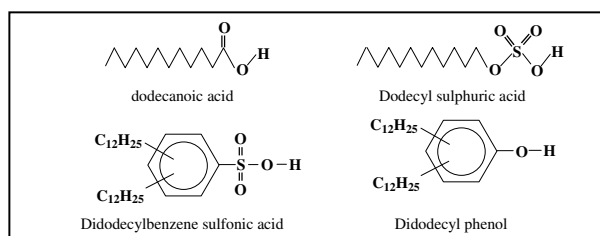
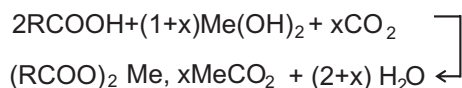
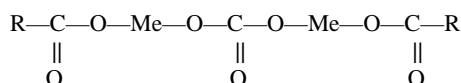


FIG. 9: Formula of four conventional organic compounds used for synthesis of amphiphilic metal salts. In the case of alkyl aryl sulfonic acids and alkyl aryl phenols, the alkyl groups (propylene tetramer) are often ramified and their location on the aromatic ring depends on the synthesis process.

overbased salts can be obtained by the following reaction [43 - 46].



In the case of Pb and Sr soaps, for $x=1$ mass spectroscopic studies allow us to determine the following molecular formula [47]:



Behaviour of the Strontium Octanoic salt micelles and overbased calcium benzene sulfonate at the liquid solid interface

As alternative ways to conventional studies, behaviours of dynamic or static aggregates at solid surfaces are investigated by means of ATEM [40, 50 - 53] and AFM experiments car-

ried out on deposits of aggregates from highly diluted dispersions (10^{-3} weight by weight) in volatile solvent (pentane). For ATEM analyses one drop of the dispersion is deposited onto a thin amorphous carbon support (15 nm thickness). For AFM studies, the dispersion is deposited onto a freshly cleaved mica surface. Experiments are carried out after total removing of the light solvent.

Figure 10 presents the ATEM results collected onto the two types of samples.

In the case of strontium octanoate micelles Electron Energy Loss Spectra (EELS) in the ranges 0 - 60 eV and 250 - 340 eV (figures 10 C and D) reveal the presence of the compound (strontium $\text{N}_{2,3}$ and $\text{M}_{2,3}$ edges) on the carbon support. The associated Energy Filtered Images (EFI figures 10 A and B) at zero loss peak and at 32 eV ($\text{Sr N}_{2,3}$) show the homogeneous spreading of strontium over the support. These results strongly suggest that strontium octanoate molecules aggregate into dynamical micelles which lead to an homogeneous molecular film when they interact with solid surfaces.

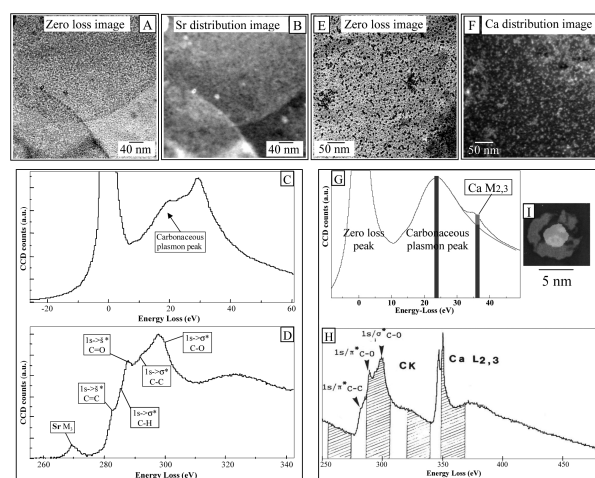


FIG. 10: EFTEM micrographs and EEL spectra recorded onto direct deposits of strontium octanoate and OCABS on thin amorphous carbon supports.

(A) (B) Zero loss and 32 eV Energy Filtered Images collected on strontium octanoate deposit showing the homogeneous spreading of strontium soap on the carbon layer.

(C) (D) EEL Spectra collected on the sample in the low loss region (0-60 eV) and middle energy range (260-340 eV) showing the presence of strontium ($\text{Sr N}_{2,3}$ and $\text{Sr M}_{2,3}$ ionization edges) and fine structures at carbon K edge characteristic of carboxylate groups ($\text{C}=\text{O}$ and $\text{C}-\text{O}$ features).

(E) (F) Zero loss and 36 eV EFIs on OCABS deposit revealing the presence of individual particles (mineral core 3 to 4 nm diameter) associated to static aggregates.

(G) (H) EEL Spectra collected on the sample in the low loss region (0-50 eV) and middle energy range (250-450 eV) showing the presence of calcium ($\text{Ca M}_{2,3}$ and $\text{Ca L}_{2,3}$ ionization edges) and fine structures at carbon K edge characteristic of carboxylate groups ($\text{C}=\text{O}$ and $\text{C}-\text{O}$ features).

(I) Composite Energy Filtered Image showing the distribution of carbon ($\text{Ef}=24$ eV in light grey) and calcium ($\text{Ef}=36$ eV in white) in an isolated particle of OCABS (6-7 nm diameter). It reveals the classical mineral core/ organic shell structure of these aggregates.

In order to support the TEM results AFM experiments were carried out on Sr octanoate deposited onto freshly cleaved

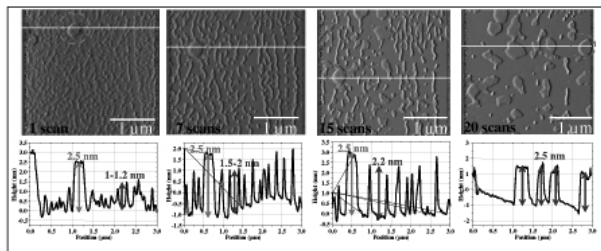


FIG. 11: AFM topographic images recorded after 1,7,15 and 20 scans on a strontium octanoate film deposited from highly diluted solution in pentane, onto a freshly cleaved mica surface. The height profiles, corresponding to the white lines in the images, allow us to deduce the size of the visualized structures.

The stable platelet surrounded by the red circle in each image is the reference object which allows us to follow the drift of the sample during the experiment and locate the height profile in the same area. The evolutions of the images and height profiles during the successive scans show that the molecules are displaced by the silicon tip and form small aggregates (1-1.2 nm size) which evolve through cylindrical, wormlike and finally lamellar assemblies (2.5 nm thickness).

mica surfaces (figure 11). At the end of the first scan, the recorded image reveals the presence of small aggregates which size, measured on the height profile, is of the order of the soap molecule length (1 to 1.2 nm).

The evolution of the recorded images as a function of scans number points out that Sr Octanoate molecules are displaced by the strain applied by the AFM tip. The shape of the aggregates progressively evolves from spherical to cylindrical, wormlike and finally lamellar assemblies. Correlatively the aggregate size increases from 1.2 nm (single molecular length) up to 2.5 nm (twice the length of the soap molecules) in the lamellar packing. Figure 12 summarizes the evolution of the molecular soap film during the AFM experiment.

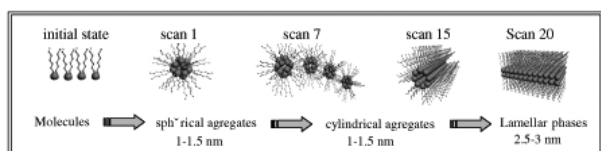


FIG. 12: Interpretation the AFM images recorded on the Sr hexanoate film deposited onto mica surface.

Before the first scan the soap molecules are homogeneously spread onto the mica surface as already revealed by EFTEM. The molecules adopt the classical brush tooth conformation. The displacement of the molecules during the tip scanning emphasizes the weak interactions of soap molecules with the mica surface. The tip induced aggregation of the molecules strongly support the dynamic character of the molecular assemblies as first revealed by ATEM investigations.

The behaviour of OCABS aggregates appears readily different. The Energy Filtered Images (figure 10 E and F) associated to the EEL Spectra in the low and middle energy loss ranges (figure G and H) show the presence on the carbon support of well separated small particles whose sizes are in the range 3-4 nm. The composite image presented in figure 10 (I) was obtained by superposition of high resolution energy filtered images at 24 eV (carbonaceous species) and 36

eV (CaL_{2,3} ionization edge) characteristic of carbonaceous (light grey blue) and calcium (white red) distribution in one single aggregate. It first reveals the classical core shell structure associated to micelles (mineral core surrounded by organic amphiphilic molecules) and seems to show the stable (static) character of these particles at the solid surface.

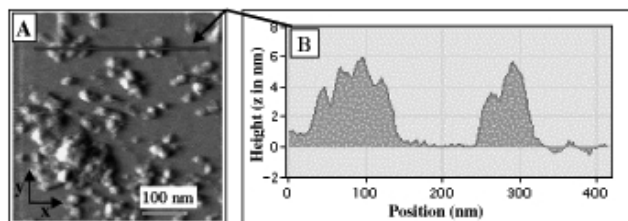


FIG. 13: (A) AFM topographic image recorded on same OCABS particles deposited onto freshly cleaved mica. (B) Height profile corresponding to the blue line in the picture allows us to deduce the particles diameter of 4 –6 nm (the particle size in the x,y image is convolved with tip radius).

The AFM results collected on a deposit of OCABS onto a freshly cleaved mica surface are presented in figure 13. OCABS aggregates appear as stable spherical particles whose sizes, deduced from the height profile lie in the range 4 to 6 nm. The static character of these aggregates is supported by the transmission micrographs presented in figure 14 on platinum shadowed replicas prepared by freeze fracturing technique on 5% OCABS in dodecane dispersion [figure 14 (a) and (b)] and on partially platinum shadowed OCABS deposits on carbon supports [figure 14 (c)]. In all cases OCABS aggregates appears as spherical particles whose cores contain calcium (EDX spectra). The structure of the mineral core has been investigated by means of Extended X rays Absorption Fine Structures [54, 55]. The results (Radial Distribution Functions) obtained on two OCABS dispersions in dodecane at Calcium K edge, using polycrystalline calcite as the standard, are presented in figure 14 (d). The presence of only one peak in the radial distribution function of the OCABS aggregates demonstrates the amorphous structure of the mineral core. The complementary ToF SIMS analyses [56] established clearly the presence of under-stoichiometric calcium carbonate amorphous phase stabilized by residual calcium hydroxide.

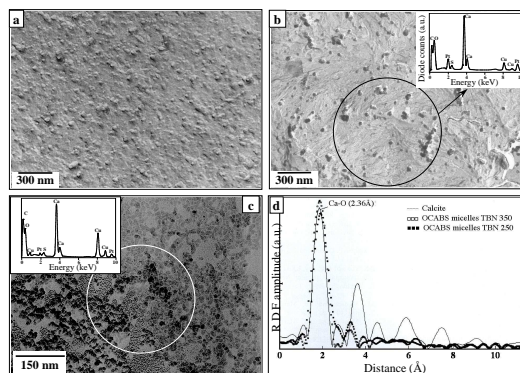


FIG. 14: TEM Micrographs recorded on platinum shadowed replica.

(a) Sample prepared on 5% dispersion of overbased calcium didodecylbenzene sulfonate in dodecane. Spherical nanoparticles of 10 nm diameters are easily visible.

(b) Extractive replica prepared on the same dispersion, (c) X ray analysis of the selected area (black circle) reveals the composition of the particles (Ca,S,O) corresponding to the sulfonate. Presence of Pt is due to the shadowing layer and copper to the copper support grid.

(c) Partially platinum shadowed sample prepared on deposits of OCABS dispersion onto thin amorphous carbon support. In the white circle shadowing and X ray analysis (D) allow us to confirm that dark grey areas are mineral core of OCABS.

(d) Radial distribution functions (from EXAFS studies) uncorrected from phase shifts obtained on calcite, and two OCABS dispersions in oil. The presence of a single peak corresponding to the first Ca-O distance points out the amorphous structure of the mineral part of the OCABS particles.

All these results are in perfect agreement with studies carried out by QELS [40], Small Angle Neutron Scattering SANS [57, 58], Small Angle X ray Scattering SAXS [59], Infra red spectroscopy (IR) [60] and Chromatography/Mass Spectroscopy-NMR (CP/MAS-NMR) [61].

reverse micelles (Sr octanoate) and amorphous carbonate encapsulated nano particles (OCABS) described in the previous sections.

Tribologic properties of the two types of colloidal systems

In order to describe the tribologic advantages of the nanolubricant approach we will focus our attention to the dynamical

System type	Compound	Formula	Aggregate shape and size
Reverse micelles (dynamic aggregates)	Strontium octanoate	$(C_7H_{15}COO)_2Sr$	Sphere Diam = 2.7 nm
Encapsulated mineral particles (static aggregates)	Overbased calcium alkyl aryl sulfonates	$(C_{24}H_{49}C_6H_4SO_3)_2Ca,(CaCO_3)_x$	Sphere Diam= 5 - 6 nm

Table 1: characteristics of the nano lubricant additives chosen as examples.

In order to simplify the tribologic results interpretation [62, 63], the colloidal additives are introduced alone in a model mineral base oil of low viscosity, normal dodecane, and the tribologic properties are evaluated using the alternative sphere

on plane tribometer presented in figure 3. The main parameters of the experiments are summarized in table 2.

Materials	Ball: 52100 AISI steel Hardness = 850 Hv Plane: 52100 AISI steel Hardness = 850 Hv
Ball diameter	9.5 mm
Roughness (Ra)	Ball: 25 nm Plane: 10 nm
Normal load	10 N
Hertz theoretical contact diameter	138 μm
Contact pressure (Hertz)	Max pressure :1 Gpa Mean pressure: 0.67 GPa
Sliding speed	3mm/s
Temperature	25°C

Table 2: experimental parameters used for the sphere / plane tribologic tests

Friction reduction and antiwear properties of Sr octanoate reverse micelles

The tribologic results recorded on Sr octanoate and OCABS dispersions in dodecane are compared to those of pure dodecane and classical ZDDP additive solution in dodecane (figure 15).

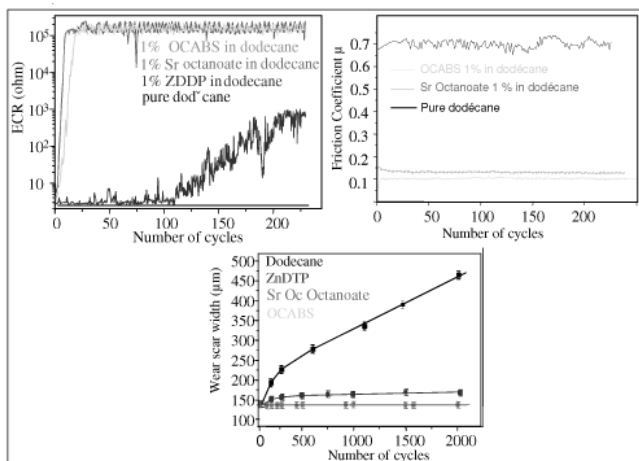


FIG. 15: Evolution of Electrical Contact Resistance (ECR), friction coefficient and wear scar width as a function of cycles number for pure dodecane, ZDDP, OCABS and Sr Octanoate in dodecane solutions.

In the case of pure dodecane, the ECR remains low (few ohms) and the friction coefficient high (0.7). The corresponding wear scar evolution shows an heavy wear characterized after 500 cycles by a wear scar depth of $0.5\mu\text{m}$ (figure 16).

In the presence of 1% ZDDP in dodecane the wear rate is high at the beginning of the experiment and reduces to a very low value after 250 cycles correlatively to the ECR stabilization (10^3 ohms) corresponding to the end of the well-known induction period necessary for the anti-wear film built up. After 500 cycles the anti-wear film is easily seen by optical microscopy and the wear scar depth is of $0.2\mu\text{m}$.

In the presence of the Sr and OCABS additives, the measured Electrical Contact Resistances are high (10^5 ohms) and friction coefficients are low ($\mu = 0.13$ for Sr additive, $\mu = 0.1$ for OCABS) as soon as the tribologic experiments start. These results emphasize the rapid built up of the triboactive phase on the surfaces at the beginning of the friction experiment. This fast built up results from physicochemical transformations, in the contact conditions, of the nano parti-

cles of additive adsorbed on the friction surfaces. The evolution of the wear rate in these two cases (figure 15) does not reveal any significant wear during the tests. The tribofilms are built on the surfaces (average thickness around $0.15 - 0.2\mu\text{m}$) and the initial surfaces polishing scratches are visible under the anti-wear film (figure 16 GH). These results clearly demonstrate the exceptional protective efficiency of such additives compared to conventional ones.

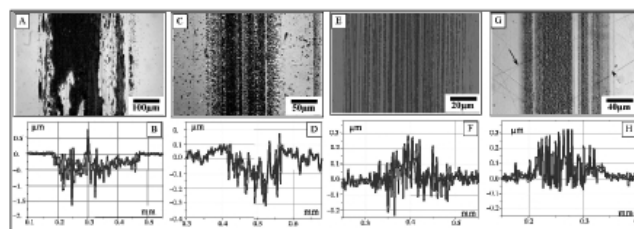


FIG. 16: Optical micrographs and surface profiles collected onto wear scars obtained after:

- 500 cycles in the presence of pure dodecane (A,B) and 1% ZDDP solution in dodecane(C,D)

- 2000 cycles in the presence of 1% dispersion in dodecane of strontium octanoate (E,F), OCABS (G,H). As it can be noticed, the tribologic film obtained (around 200 nm thick) in the presence of nano sized additives is built on the initial surfaces whereas in the presence of dodecane or ZDDP, the wear scars have respectively 500 and 200 nm of depth. It is important to note that, in the case of nano-additives, the polishing scratches of the initial surfaces are easily seen (arrows in G) under the partially transparent anti wear film. This fact points out that there is no significant wear (down to few nm) in the presence of the chosen colloidal additives.

Nature and structure of anti-wear films obtained with strontium and calcium compounds

In order to complete the understanding of the action mechanisms of colloidal additives the nature and structure of anti-wear films obtained in the presence of two representative systems (Sr octanoate dynamic micelles and OCABS particles) are investigated by means of Analytical Transmission Microscopy the main results being presented in figure 17 and 18.

The two anti-wear films present polycrystalline structures as clearly pointed out by the electron diffraction patterns which present well defined Debye - Sherrer rings. Indexations of these last ones reveal that micro-crystals are mainly

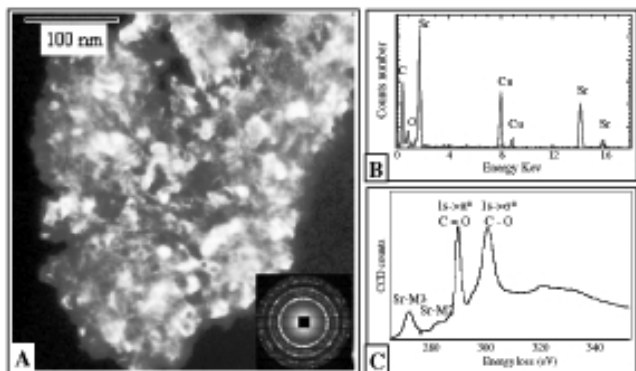


FIG. 17: Dark field transmission electron micrograph and selected area electron diffraction pattern recorded on a tribological film particle obtained in the presence of Sr octanoate micelles.

The indexing of the electron diffraction pattern allowed us to conclude that the tribofilm is made of polycrystalline strontianite, the size of the crystallites lying in the range 10-150 nm.

The EDX spectrum does not evidence the presence of iron underlining the high anti-wear properties and the absence of chemical reaction with the substrate for the built up of the tribofilm (copper peaks are due to support grid).

The EEL spectrum at carbon K ionization edge mainly reveals the fine structures characteristic of carbonate groups. This indicate that hydrocarbon chains are not significantly present in the film.

carbonate phases, respectively strontianite (Sr octanoate additive) and calcite (OCABS).

In the case of the OCABS film, electron micro-diffraction patterns carried out between well-identified nano-crystallites demonstrate the existence of an amorphous phase responsible of the cohesion of the film. This phase, not identified by ATEM probably corresponds to (amorphous) calcium oxide species recently detected by ToF SIMS analyses [64].

The EEL spectra collected at carbon K edge on the two films (Figure 17C and 18D) present great differences with the corresponding spectra in the initial additives. The fine structures associated to C=C, C-C and C-H bondings in the initial compounds are not significantly detected in the EEL spectra of the films. These last ones are dominated by the well known fine structures associated to C=O and C-O [52, 62]. These results demonstrate that hydrocarbon chains are no more significantly present in the films implying their quite total elimination during the friction process.

The absence of iron in the tribo-film as revealed by EDXS spectra collected on the two films (figure 17B and 18C) strongly supports that chemical reactions between the nano additives and the substrates are not involved in the anti-wear film formation. It confirms that induction period is not needed for the tribofilm establishment and then points out the high protective efficiency against wear of such nano-additives.

A significant difference of behaviour for the two additives is evidenced by the size of the micro crystals present in the respective films. In the case of OCABS the micro crystals have dimension ($\sim 6 - 10\text{nm}$) close to the mineral core of the initial particles (5-7 nm). The crystals present in the strontianite film are readily larger ($\sim 10 - 150\text{nm}$) than initial micelle's cores (1nm) involving a more complex re-crystallisation process.

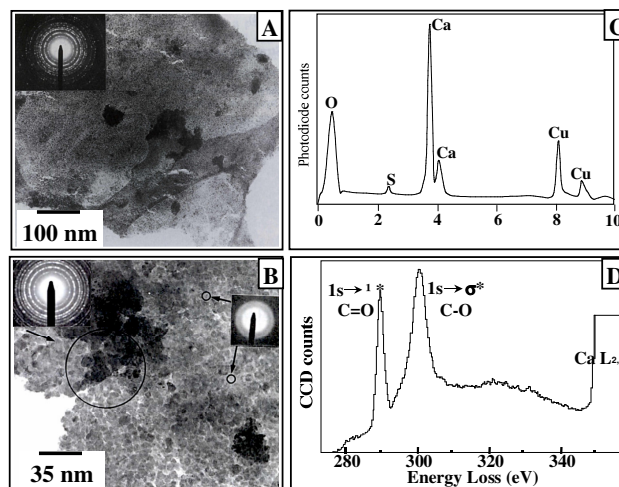


FIG. 18: (A) and (B), transmission electron micrographs and electron diffraction patterns recorded on tribological film particles obtained in the presence of OCABS in dodecane dispersion.

(C), (D) corresponding EDX and EELS spectra. The film is composed of nano-crystallites of calcite (diffraction) which average size is 10 nm aggregated by means of ill ordered areas (diffuse diffraction). EDX spectrum reveals that iron is not detected (copper peaks are due to the support grid). EEL spectrum at Carbon K edge is dominated by carbonate fine structures and points out that hydrocarbon chains are not significantly detected in the film.

Associated antifriction and anti-wear actions in tribologic behaviour of colloidal additives

The examples chosen to illustrate the tribologic behaviour allow us to draw the various actions of such colloidal additives.

The friction reduction is mainly attributed to the adsorption film of additive (organic molecule, soap molecules or encapsulated particles). The length of the organic shell (organic chains) is a first order parameter according to Zisman experiments (as large is the chain as low is the friction coefficient). The exceptional wear reduction in the wear test is associated to the quasi-instantaneous built up of a stable tribologic film from the adsorbed additive layer. The polycrystalline carbonate nature of the film results from the elimination of part of the organic radicals(oxidization) and the crystallization of ill organized cores of the micelles or encapsulated particles under the physical conditions of the sliding contact ($P \approx 1\text{GPa}$, shear stress $\approx 10^5\text{s}^{-1}$, oxidative species, flash temperatures. . .).

It is important to note that the carbonate phases produced in the sliding contact does not present excellent friction reduction properties if used as solid lubricants. Recent experiments [65] demonstrated that a friction coefficient of 0.6 is obtained with surface films of pure polycrystalline calcite. This coefficient reduces to 0.06 when pure dodecane is added or to 0.1 in the presence of Octanoic acid molecules. These results emphasize the role of the amphiphilic molecules in the inter crystallite interactions responsible of the mechanical behaviour of the nano-granular tribo-films.

As a conclusion the action of the colloidal additives studied can be described as follows:

Step 1: adsorption of the additive on the substrate surfaces

Step 2: loss of hydrocarbon chains and crystallization of the mineral part of the colloids under the physico-chemical conditions of the sliding contact ($P \approx 1 \text{ GPa}$, shear stress $\approx 10^5 \text{ s}^{-1}$, flash temperature, oxidizing species...).

These transformations do not imply any chemical reaction with surfaces components

Step 3: the tribofilm is worn instead of metal substrates (substitution wear) and regenerated from additive molecules or aggregates adsorbed on its surface.

The role of amphiphilic molecules of the organic surrounding shell is to reduce friction either by adsorption on the surface film or by modifying (lowering) the inter-grains interactions.

The anti-wear action works via substitution wear of the tribochemical film. This one is continuously regenerated from the additive adsorbed layer. The consumption of additive (apart from the initial adsorption on the whole surfaces) is se-

lectively located in the sliding contact due to the fact that the anti-wear film built up needs the physicochemical conditions of the sliding contact to operate.

II. CONCLUSION AND PERSPECTIVES

Colloidal physics and chemistry offer interesting ways of research in the reduction of friction and wear applied to various metallurgical contexts. The development of additives that do not involve reaction with contacting substrates and the possibilities to associate in the same colloidal particle corrosion inhibition, friction reduction and anti wear actions are of great interest.

The chemical methods developed in order to produce nano-sized dynamic or static particles will allow the tribologist to design stable dispersion in oil of selected compounds precursors of efficient tribochemical film.

-
- [1] D. DOWSON, "History of Tribology, Longmans, London, (1979).
- [2] G. AMONTON, Mémoires de Mathématiques et de Physique de l'Académie Royale des Sciences, p. 206, (1999).
- [3] C.A. COULOMB, Mémoires de Mathématiques et de Physique de l'Académie Royale des Sciences, p. 161, (1785).
- [4] H. HERTZ, "Über die Berührung fester elastischer Körper", J. reine und angewandte Mathematik, 92, p. 156-171, (1882)
- [5] R. STRIBECK, Die Wesentlichen Eigenschaften der Gleit- und Rollenlager, Z. Verein. Deut. Ing. Vol. 46 n°38, p. 1341-1348, (1902).
- [6] Sir W.B. HARDY, Collected works, University Press, Cambridge, (1936).
- [7] K.L. JOHNSON, Contacts mechanics, Cambridge University Press, Cambridge, (1985).
- [8] W.A. ZISMAN, "durability and wettability properties of monomolecular films on solids", friction and wear, R. DAVIES (Ed), Elsevier, Amsterdam, p110-148 (1959).
- [9] A.S. AKHMATOV, Molecular Physics of Boundary Friction, IPST, Jerusalem, (1966).
- [10] J.M. MARTIN, Contribution à la tribologie: Etude du mécanisme d'action d'un additif anti-usure en regime de lubrification limite. Aspects chimiques dans le cas des organodithiophosphates métalliques, Thèse d'état n° 7827, Université Claude Bernard, Lyon, (1978).
- [11] J.M. MARTIN, J.L. MANSOT, I. BERBEZIER, H. DEXPERT, "The nature and origin of wear particle from boundary lubrication with ZDDP", Wear, 93 (2), p. 117-126, (1984).
- [12] J.M. MARTIN, J.L. MANSOT, I. BERBEZIER, M. BELIN, "Microstructural aspects of lubricated mild wear with zinc dithiophosphate", Wear, 107, p. 355-366, (1986).
- [13] J.M. MARTIN, M. BELIN, J.L. MANSOT, "Friction induced amorphization with ZDDP. An EXAFS study", ASLE Transactions, 49(4), p. 523-531, (1986).
- [14] M. BELIN, J.M. MARTIN, J.L. MANSOT, "Role of iron in the amorphization process in friction-induced phosphate glasses", Journal de Physique, 48(C9), p. 1147-53 (1987).
- [15] J.C. BELL, K.M. DELARGY, A.M. SEENEY, "the removal of substrate material through thick zinc dithiophosphate anti-wear films". In D. DOWSON et al., editors. Tribology series, 21, wear particles: from the cradle to the grave. Amsterdam. Elsevier; p. 387-96, (1992).
- [16] J.M. MARTIN, C. GROSSIORD, T. LEMOGNE, S. BEC, A. TONCK, "The two layers structure of ZnDTP tribofilm part 1: AES, XPS and XANES analyses". Tribol. Int., 31(10), p. 627-44, (2001).
- [17] H. SPIKES, "The history and mechanisms of ZDDP". Tribol. Lett., 17 (3), p. 469-89, (2004).
- [18] J.M. MARTIN, "Lubricant additives and the chemistry of rubbing surfaces: metal dithiophosphates triboreaction films revisited". Jpn. J. Tribol. 42, p9, (1997).
- [19] J.M. MARTIN, "Antiwear mechanisms of zinc dithiophosphate: a chemical hardness approach". Tribol. Lett., 6, p.1- 8, (1999).
- [20] W. HIRST and A.J. MOORE, Proc. Roy. Soc. Lond., A 365, p. 537-565, (1979).
- [21] J.L. MANSOT, "Aspect microscopique de l'action des reduceurs de frottement en lubrification limite", Docteur Ingenieur Thesis, Ecole Centrale de Lyon, (1982).
- [22] J.L. MANSOT, J.M. MARTIN, "In situ measurements of thickness thin variations of boundary films by means of tunneling conductivity", proceedings of the Leeds-Lyon Symposium, (1983).
- [23] G.A. TOMLINSON, Phil. Mag. Ser., 7, p. 905, (1929).
- [24] P. BILAS, L. ROMANA, F. BADE, K. DELBE, and J.L. MANSOT, "Speed and atmosphere influences on Nanotribological properties of NbSe2", Tribology Letters, vol 34 n°1, p41, (2009).
- [25] S.N. POSTNIKOV, Electrophysical and electrochemical phenomena in friction, cutting and lubrication p. 113-114, Van Nostrand Reinhold comp., London, (1978).
- [26] J.M. GEORGES and T. MATHIA, J. Mech. Appl., vol.2, p 231-266, (1978).
- [27] J.L. MANSOT, V. GOLABKAN, L. ROMANA, Ph. BILAS, E. ALLEMAN, Y. BERCIION, "Tribological and physicochemical characterization of strontium colloidal additives in mild wear regime", Coll. and Surf. A, vol. 243, p67, (2004).
- [28] S. COHEN, L. RAPOPORT, E. A. PONOMAREV, H. COHEN, T. TSIRLINA, R. TENNE, and C. LEVY-CLEMENT, "the tribological properties of typeII texturated MX2 (M=Mo,

- W; X=S,Se)", *Thin Solid Films*, vol. 324, p. 190, (1998).
- [29] R. TENNE, M. HOMYONFER, and Y FELDMAN, "Nanoparticles of layered compounds with hollow cage structures, *Chemistry of materials*", vol 10(11), p. 3225, (1998).
- [30] P. THOMAS, K. DELBE, D. HIMMEL, J.L. MANSOT, K. GUERIN, M. DUBOIS, C. DELABARRE, A. HAMWI, "Tribological properties of low-temperature graphite fluorides. Influence of the structure on the lubricating performances", *J. Phys. Chem. Solids*, vol. 67, n° 5-6, p. 1095, (2006).
- [31] L. RAPOPORT, Y. FELDMAN, M. HOMYONFER, H. COHEN, J. SLOAN, J.L. HUTCHISON, and R. TENNE, "Inorganic fullerene like materials as additives to lubricants: structure-function relationship", *Wear*, vol. 225-229, p. 975, (1999).
- [32] L. RAPOPORT, Y. BILIK, Y. FELDMAN, M. HOMYONFER, S.R. COHEN and R. TENNE, "Hollow nano-particles of WS₂ as potential solid state lubricants, *Nature*, vol. 387, p. 791, (1997).
- [33] J.J. HU and J.S. ZABINSKI, "Nanotribology and lubrication mechanisms of inorganic fullerene like MoS₂ nanoparticles investigated using lateral Force Microscopy", *Tribology letters*, vol. 18 (2), p. 173, (2005).
- [34] L. JOLY-POTTUZ, F. DASSENOY, M. BELIN, B. VACHER, J.M. MARTIN, and N. FLEISHAUER, "Ultra low friction and wear properties of IF-WS₂ under boundary lubrication, *Tribology letters*, vol. 18 (4), p. 477, (2005).
- [35] P. Thomas, K. Delbe, D. Himmel, J.L. Mansot, M. Dubois, K. Guerin, W. Zhang, A. Hamwi, "Tribological properties of fluorinated carbon nanofibres", *Tribology Letters*, vol.34 n°1, p.49, (2009).
- [36] J.L. MANSOT, K. DELBE, P. THOMAS, "tribo-synthesis of graphite Lithium intercalated compounds", proceedings of the Am. Chem. Soc. Meeting, New Orleans, (2008).
- [37] D. LANGEVIN in P.L. LUISI and B.E. STRAUB (Eds.), "Reverse Micelles", Plenum, New York, p.287, (1982).
- [38] K.L. MITTAL and P. MUKERJEE, "The wide world of micelles", *Micellization, Solubilization and Microemulsions* vol. 1, K.L. MITTAL (Ed.), Plenum, New York, p1-22, (1977).
- [39] H.F. EICKE, "Micelles in apolar media", *Micellization, Solubilization and Microemulsions* vol. 1, K.L. MITTAL (Ed.), Plenum, New York, p. 429-444, (1977).
- [40] R. MAKLOUFHI, J.L. MANSOT, E. HIRSH, J. WERY, S.J. CANDAU, J.P. THOMAS and J.P. ROLLAND, "Electron Microscopy and Light Scattering Study of Organometallic Inverse Micellar Systems", *Colloid & Polymer Science*, 273, p. 242, (1995).
- [41] J.L. MANSOT, J.M. MARTIN, S.J. CANDAU, "Amphiphilic complex ester as lubricant additive. Part one : Structure of paraffinic solutions", *Coll. and Surf.*,7, p. 301, (1983).
- [42] E.L. BENEDETTI and P. FAVARD, "Freeze Etching Techniques and applications", *Société Française de Microscopie Electronique*, (1973).
- [43] MARTIN, MANSOT, HURIER et MAROTEL, "Savons de calcium possédant une réserve de basicité élevée", international patent n° 85/19393, (1985).
- [44] J.R. WITTLE, "Method of preparing overbased calcium sulfonates", US patent n° 4,427,559 (1984).
- [45] C.BELLE et al, "Mécanismes des réactions polyphasiques: cinétique de formation de carbonate de calcium colloidal en milieu apolaire", *J. Chim. Phys.*, 87, p.93-104 (1990).
- [46] L.K. HUDSON, J. EASTOE and P.J. DOWDING, "Nanotechnology in action : overbased nanodetergent as lubricant oil additives", *Advances in Coll. and Interf. Sci.*, 123-126, p.425-431, (2006).
- [47] J. WERY-VENTURINI, "contribution à l'étude de la structure microscopique de micelles inverses d'octanoate de plomb", Thèse de doctorat, Université de Nantes (1992).
- [48] J. WERY and J.L. MANSOT, "Quantitative study of irradiation damage in organometallic colloidal particles", *Microsc. Microa. Microstruc.*, vol. 4, n° 1, (1993).
- [49] J.L. MANSOT, J. WERY and P. LAGARDE, "Local Structure Analysis of the mineral core of reverse micelles in dispersion in Hydrocarbons", *Colloids and Surfaces*, 90, p.167-182, (1994).
- [50] J.M. MARTIN, J.L. MANSOT and M. HALLOUIS, "Energy filtered electron microscopy (EFEM) of overbased calcium alkylaryl sulfonate micelles", *Ultramicroscopy*, 30, p. 321-328, (1990).
- [51] J.M. MARTIN, J.L. MANSOT, M. HALLOUIS and H. TENAILLEAU, "High Resolution Electron Spectroscopic Imaging (ESI) of Reverse Micelles", *Microscopy, Microanalysis, Microstructure*, 2,p.1-8, (1990).
- [52] J.L. MANSOT, M. HALLOUIS and J. M. MARTIN, "Colloidal antiwear additives Part One : Structural study of overbased calcium alkylbenzene sulfonate micelles", *Colloids and Surfaces A*, 71, p. 123-134, (1993).
- [53] J.L. MANSOT, V. GOLABKAN, L. ROMANA, Th. CESAIRE, "Chemical and physical characterization by EELS of strontium hexanoate reverse micelles and strontium carbonate nanophase produced during tribological experiments", *J. of Micr.*, vol. 210, p. 110, (2003).
- [54] J.M. MARTIN, M. BELIN, J.L. MANSOT, "EXAFS of calcium in overbased micelles", *Journal de Physique*, vol. 12 n° 47, p. 887-890, (1986).
- [55] J.L. MANSOT, J.M. MARTIN, H. DEXPERT, D. FAURE, P. HOORNAERT and R.GALLO, "Local structure analysis in overbased reverse micelles", *Physica B*,158, p. 237 (1989).
- [56] L. CISAIRE, J.M. MARTIN, T. LEMOGNE and E. GRESSER, "Chemical analysis of overbased calcium sulfonate detergents by coupling XPS, Tof-SIMS, XANES and EFTEM, *Coll. and Surf. A:Physicochem. Eng.Aspects*, 238, p.151-158, (2004).
- [57] I. MARKOVIC, R.H. OTTEWILL, D.J. CEBULA, I. FIELD and J.F. MARSH, "Small angle neutron scattering studies on non aqueous dispersions of calcium carbonate Part 1 Guinier approach", *Colloid and Polym. Sci.*, 262, p.648 (1984).
- [58] I. MARKOVIC, R.H. OTTEWILL, D.J. CEBULA, I. FIELD and J.F. MARSH, "Small angle neutron scattering studies on non aqueous dispersions of calcium carbonate Part 2", *Colloid and Polym. Sci.*, 264, p.265-276 (1986).
- [59] S. GIASSON, D. ESPINAT, T. PALERMO, R. OBER, M. PESSAH and M. F. MORIZUR, "Small angle X-Ray scattering (SAXS) on calcium sulfonate dispersions: effects of friction on microstructure", *J. of Coll. and Interf. Sci.*, 153(2), p. 355-367, (1992).
- [60] S. GIASSON, T. PALERMO, T. BUFFETEAU, B. DESBAT and J. M. TURLET, "Study of boundary film formation with overbased calcium sulfonate by PM-IRRAS spectroscopy", *Thin Solid Films*, 252, p. 111-119, (1994).
- [61] E. R. ARNDT and K. L. KREUZ, "Characterization of calcium alkylaryl sulfonates containing encapsulated solids", *J. of Coll. and Interf. Sci.*, 123, p. 230-237, (1988).
- [62] J.L. MANSOT, M. HALLOUIS and J.M. MARTIN, "Colloidal antiwear additives - Part two : Tribological behaviour of colloidal additives in mild wear regime", *Colloids and Surfaces A*, 75, p. 25-31, (1993).
- [63] J.L. MANSOT, V. GOLABKAN, L. ROMANA, Ph. BILAS, E. ALLEMAN, Y. BERCION, "Tribological and physicochemical characterization of strontium colloidal additives in mild wear regime", *Coll. and Surf. A*, vol. 243, p. 67 (2004).
- [64] T. KUBO, S. FIJIWARA, H. NANA O I. MINAMI, S. MORI, "Tof-SIMS analysis of boundary films derived from calcium

sulfonates“, *Tribo. Lett.*, 23(2), p.171-176,(2006).
[65] J.L. MANSOT, ”Nanolubrication, the colloidal approach”,

STLE annual meeting, Cleveland , USA, (mai 2008).